1330 *Chem. Mater.* **2010,** *22,* 1330–1339
DOI:10.1021/cm901771y

CHEMISTRY OF MATERIALS
Article

Structure−Property Relationships for Methylsilsesquioxanes

Hyun Wook Ro,*[,†,‡] Eun Su Park,[†] Christopher L. Soles,*[,‡] and Do Y. Yoon*[,†]

[†]*Department of Chemistry, Seoul National University, Seoul 151-747, Korea and* [‡]*Polymers Division, National Institutes of Standards and Technology, Gaithersburg, Maryland 20899*

Received June 24, 2009. Revised Manuscript Received November 24, 2009

Critical structure−property relationships are delineated for a widely used class of methylsilsesquioxane (MSQ) materials. We obtained a range of MSQ prepolymers with different microstructures by varying the synthetic conditions. The structure of such different oligomers were measured and correlated with the physical properties of final (thermally cured) MSQ films. The microstructural analysis was performed using a combination of graphite plate laser desorption/ionization time-of-flight mass spectrometry (GPLDI-TOF MS), size exclusion chromatography (SEC), and Fourier transform infrared spectroscopy (FT-IR). These measurements show that, as the MSQs grow in size, the propensity to form closed cage-type architectures is higher for molecular masses below 1000 u. When these prepolymers are spin-cast into thin films and thermally cured (vitrified) into final organosilicate polymers, the cage-type microstructures have detrimental effects on the physical properties of the film. They result in films with poor optical quality and a very large coefficient of thermal expansion. The structural basis for these variations in the physical properties is discussed in detail.

Introduction

Silsesquioxanes (SSQs) are utilized in thin films or coatings for a range of applications, including nanocomposites,[1,2] scratch resistant coatings,[3] barrier coatings,[4] biological devices,[5,6] separation media,[7] optical films or coatings,[8] and semiconductor interconnect insulators.[9−16] Some of their attractive attributes includes the ease with which SSQs can be processed into high quality films and coatings, the ability of these films and coatings to support high levels of porosity, and their ability to resist high temperatures and aggressive chemical environments without degradation. However, it is also difficult to obtain reproducible and well-controlled bounds on the physical properties of these SSQ materials. Their performance can vary significantly with the synthetic conditions or processing parameters. The objective of this paper is to address this variability in the physical properties and elucidate the molecular/microstructural basis for these variations in methylsilsesquioxanes (MSQs), one of the most common SSQ type materials. A better understanding of how to tune and control the properties provides materials developers the tools to rationally improve the performance and properties of MSQ type materials.

In their final state, MSQs are highly cross-linked siloxane networks with one nonreactive methyl group per Si atom and are typically synthesized from trifunctionalsilane monomers such as methyltrialkoxysilanes or methyltrichlorosilane.[17−19] When these silanes are hydrolyzed in the presence of acidic or basic catalysts and H_2O, reactive silanol (Si−OH) groups are formed. A condensation reaction between two silanols then leads to a siloxane (Si−O−Si) linkage, through either intermolecular or intramolecular condensation reactions. Here, the trifunctionalsilane

*To whom correspondence should be addressed: hyun.ro@nist.gov (H.W.R.); csoles@nist.gov (C.L.S.); dyyoon@snu.ac.kr (D.Y.Y.).

(1) Kannan, R. Y.; Salacinski, H. J.; Butler, P. E.; Seifalian, A. M. *Acc. Chem. Res.* **2005**, *38*, 879.
(2) Choi, J.; Yee, A. F.; Laine, R. M. *Macromolecules* **2004**, *37*, 3267.
(3) Laine, R. M.; Roll, M.; Asuncion, M.; Sulaiman, S.; Popova, V.; Bartz, D.; Klug, D. J.; Mutin, P. H. *J. Sol-Gel Sci. Technol.* **2008**, *46*, 335.
(4) Asuncion, M. Z.; Laine, R. M. *Macromolecules* **2007**, *40*, 555.
(5) Kim, H.-C.; Wallraff, G.; Kreller, C. R.; Angelos, S.; Lee, V. Y.; Volksen, W.; Miller, R. D. *Nano Lett.* **2004**, *4*, 1169.
(6) Kim, H.-C.; Kreller, C. R.; Tran, K. A.; Sisodiya, V.; Angelos, S.; Wallraff, G.; Swanson, S.; Miller, R. D. *Chem. Mater.* **2004**, *16*, 4267.
(7) Dong, H.; Brook, M. A.; Brennan, J. D. *Chem. Mater.* **2005**, *17*, 2807.
(8) Chen, W.-C.; Lee, L.-H.; Chen, B.-F.; Yen, C.-T. *J. Mater. Chem.* **2002**, *12*, 3644.
(9) Nguyen, C. V.; Carter, K. R.; Hawker, C. J.; Hedrick, J. L.; Jaffe, R. L.; Miller, R. D.; Remenar, J. F.; Rhee, H.-W.; Rice, P. M.; Toney, M. F.; Trollsas, M.; Yoon, D. Y. *Chem. Mater.* **1999**, *11*, 3080.
(10) Miller, R. D. *Science* **1999**, *286*, 421.
(11) Maex, K.; Baklanov, M. R.; Shamiryan, D.; Iacopi, F.; Brongersma, S. H.; Yanovitskaya, Z. S. *J. Appl. Phys.* **2003**, *93*, 8793.
(12) Landskron, K.; Hatton, B. D.; Perovic, D. D.; Ozin, G. A. *Science* **2003**, *302*, 266.
(13) Pai, R. A.; Humayun, R.; Schulberg, M. T.; Sengupta, A.; Sun, J.-N.; Watkins, J. J. *Science* **2004**, *303*, 507.
(14) Yang, S.; Mirau, P.; Pai, C. S.; Nalamasu, O.; Reichmanis, E.; Pai, J. C.; Obeng, S. Y.; Seputro, J.; Lin, E. K.; Lee, H.-J.; Sun, J.; Gidley, D. W. *Chem. Mater.* **2002**, *14*, 369.
(15) Ro, H. W.; Kim, K. J.; Theato, P.; Gidley, D. W.; Yoon, D. Y. *Macromolecules* **2005**, *38*, 1031.
(16) Kohl, A. T.; Mimna, R.; Shick, R.; Rhodes, L.; Wang, Z. L.; Kohl, P. A. *Electrochem. Solid-State Lett.* **1999**, *2*, 77.
(17) Baney, R. H.; Itoh, M.; Sakakibara, A.; Suzuki, T. *Chem. Rev.* **1995**, *95*, 1409.
(18) Abe, Y.; Hatano, H.; Gunji, T. *J. Polym. Sci., Part A: Polym. Chem.* **1995**, *33*, 751.
(19) Lee, J.-K.; Char, K.; Rhee, H.-W.; Ro, H. W.; Yoo, D. Y.; Yoon, D. Y. *Polymer* **2001**, *42*, 9085.

Published on Web 01/07/2010

monomers, each containing one Si atom, assemble into higher molecular mass products with a range of distinctly different topologies or cross-link architectures. One extreme is a ladder network where the Si atoms form the junctions of the ladder and the O atoms comprise the rungs and struts of the ladder. The other extreme would be a polyhedral oligomeric silsesquioxane (POSS), like the octamethyl-T_8 cube, where eight Si atoms reside at the corners of the cube and the O linkages connect the corners. In this octamethyl-T_8 cube, the nonreactive methyl vertices isolate the cube from the rest of the cross-linked network. In reality, trifunctionalsilanes condense into a breadth of microstructures, ranging from the closed cage structures involving six or more Si atoms (T_n, where $n \geq 6$), to partial or incomplete cages with residual Si−OH groups ($T_n(OH)_m$), and finally to high branched ladder-like networks.[17−21] In this manuscript we demonstrate how measuring and then rationally controlling the evolution of the microstructure of this cross-linked network is important for tuning the physical properties of the final MSQ material.

MSQs have received considerable attention in the organosilicate glass (OSG) literature as a promising candidate for ultralow-dielectric constant (ultralow-k, $k < 2.2$) interlayer dielectric (ILD) insulator materials for next generation semiconductor interconnects.[14−16] However, the mechanisms by which the microstructure of the cross-linked network evolves in this material is poorly understood. Compared with SSQs where the organic substituent is larger than a methyl group, the reaction rates in the MSQ are relatively fast and lead to structural complexity. Others have studied the structural rearrangement and thermal stability of MSQ materials during thermal curing/vitrification process with Fourier transform-infrared (FT-IR) spectroscopy.[22−24] These measurements suggest that the physical properties of the fully vitrified film, such as the refractive index, dielectric constant, and mechanical properties, depend on the microstructure of initial spin-cast MSQ.[25] However, the microstructure of the initial products and the detailed nature of their transformation during thermal curing are still not understood well.

We recently reported theoretical and experimental FT-IR spectroscopy investigations of the microstructure evolution in a series of SSQ materials.[26] It was shown that the different microstructures can be distinguished from their Si−O−Si stretching modes in the vibrational density of states, from both theoretical calculations and experimental FT-IR data; excellent agreement was observed between the experiment and theory. Consistent with the published results in the field, it was also shown that the secondary condensation reaction during thermal vitrification induces structural transformation from partial cage or nearly perfect cage structures toward a random network structures with lower symmetry.

On a similar front we have also reported on high-modulus thin films of MSQ-like copolymers synthesized from methyltrimethoxysilane (MTMS) and 1,2-bis-(triethoxysilyl)ethane (BTSE).[27] The BTSE monomer is like the MTMS with the exception that the terminal methyl group is replaced with an ethylene bridge covalently connected to another trifunctionalsilane. Significant improvements in the physical properties such as modulus, hardness and coefficient of thermal expansion (CTE) were observed as the mole fraction of BTSE increases. A microstructural analysis showed that BTSE plays the decisive role to create closed cage structures that retain the functional silanol groups and can continue to react with the rest of the cross-linked network; without BTSE, the perfect closed cage structures become isolated and cannot be covalently linked to the rest of the network. The isolated cage structures formed without BTSE lead to a degradation of the film properties after the vitrification at elevated temperatures where these nonbonded cages evaporate or sublime, leaving a loosely cross-linked network of low density. This study demonstrated how the film properties can be tuned by tailoring the initial microstructures of MSQ-type OSG materials.

In this study, we focus on pure MSQ, which is an attractive OSG from an application point of view, and provide valuable information about the microstructural development and its relationship to the thin film properties. The MSQs are again synthesized from the common MTMS, and their molecular masses are determined under varying reaction time and temperature conditions. The microstructure of the initial low molecular-mass MSQs are characterized in terms of the cage and/or branching content through a combination of size exclusion chromatography (SEC) and graphite plate laser desorption ionization time-of-flight mass spectrometry (GPLDI-TOF MS). The structural transformation of these MSQ prepolymers into hard OSGs upon thermal vitrification is characterized by FT-IR spectroscopy and thermogravimetric analysis (TGA) as a function of the vitrification temperature. Finally, the essential physical properties such as average film density, wall density, porosity, and CTE of different MSQ films are determined by specular X-ray reflectivity (SXR) and X-ray porosimetry (XRP), and interpreted in terms of the initial microstructure and the structural transformation during the vitrification process.

Experimental Section

Materials. The MTMS was obtained from Lancaster Synthesis [Certain commercial materials and equipment are identified

(20) Kim, H.-J.; Lee, J.-K.; Park, S.-J.; Ro, H. W.; Yoo, D. Y.; Yoon, D. Y. *Anal. Chem.* **2000**, *72*, 5673.
(21) Franco, R.; Kandalam, A. K.; Pandey, R.; Pernisz, U. C. *J. Phys. Chem. B* **2002**, *106*, 1709.
(22) Chen, W. C.; Lin, A. C.; Dai, B. T.; Tsai, M. S. *J. Electrochem. Soc.* **1999**, *146*, 3004.
(23) Wang, C. Y.; Shen, Z. X.; Zheng, J. Z. *Appl. Spectrosc.* **2000**, *54*, 209.
(24) Wang, C. Y.; Shen, Z. X.; Zheng, J. Z. *Appl. Spectrosc.* **2001**, *55*, 1347.
(25) Lee, L.-H.; Chen, W.-C.; Liu, W.-C. *J. Polym. Sci., Part A: Polym. Chem.* **2002**, *40*, 1560.
(26) Park, E. S.; Ro, H. W.; Nguyen, C. V.; Jaffe, R. L.; Yoon, D. Y. *Chem. Mater.* **2008**, *20*, 1548.
(27) Ro, H. W.; Char, K.; Jeon, E.-c.; Kim, H.-J.; Kwon, D.; Lee, H.-J.; Lee, J.-K.; Rhee, H.-W.; Soles, C. L.; Yoon, D. Y. *Adv. Mater.* **2007**, *19*, 705.

in this paper in order to specify adequately the experimental procedure. In no case does such identification imply recommendation by the National Institute of Standards and Technology nor does it imply that the material or equipment identified is necessarily the best available for this purpose.] and used as received, without further purification. THF was distilled from sodium/benzophenone under nitrogen and used as the solvent. The MSQs were prepared through a hydrolytic condensation of the MTMS in the presence of HCl [R_1 (mol of HCl/mol of MTMS) = 0.03] and an excess of H_2O [R_2 (mol of H_2O/mol of MTMS) = 10.0.] under a nitrogen atmosphere. The mass of the MTMS with respect to the total mass of the reaction mixture was 40% [(mass of MTMS/(mass of MTMS + mass of THF)) × 100]. Three different MSQ samples were prepared under the following conditions: MSQ-1 at 40 °C for 30 min, MSQ-2 at 40 °C for 24 h, MSQ-3 at 60 °C for 24 h. The solutions were then diluted with copious amounts of methyl-isobutylketone (MIBK). After washing at least 3 times with water, the organic phase was dried with $MgSO_4$, filtered, and solvent was evaporated in vacuum. The product obtained after vacuum-drying was either a colorless viscous liquid (MSQ-1) or a white solid powder (MSQ-2 and 3). The products were then dissolved in 4-methyl-2-pentanone (MIBK) at a concentration of 30% by mass, filtered through a 0.2 μm PTFE syringe, and dispensed onto Si wafers precleaned with a piranha solution (volume ratio of H_2SO_4:H_2O_2 equal to 7:3). These substrates were spun at (209 to 314) rad/s for 60 s into smooth films and then thermally vitrified into hard OSG materials by heating the spin-cast samples to 430 °C at a rate of 3 °C/min under vacuum.

Size Exclusion Chromatography (SEC). SEC was performed on a chromatogram consisting of two mixed-bed Jordi columns with a dual-detector system comprised of a Waters 2410 differential refractometer and a Viscotek 270 detector. The MSQs were added to THF at a concentration of 0.5% by mass and pumped through the columns at a flow rate of 1.0 mL/min. The column was calibrated using polystyrene standards (Polymer Standard Service, Inc.) ranging in weight average mass from 500 to 1 000 000 Da.

Fourier Transform Infrared (FT-IR) Spectroscopy. Transmission FT-IR spectra of the thin films on Si-wafers were obtained on a JASCO FT-IR spectrometer (660 Plus equipment) using 4 cm^{-1} spectral resolution, averaging each spectra over 512 scans. FT-IR spectra were obtained from the as-cast MSQ films and as a function of temperature through the vitrifcation process. Data collection was repeated at least three times in order to confirm the reproducibility.

Graphite Plate Laser Desorption Ionization Time-of-Flight Mass Spectroscopy (GPLDI-TOF MS). The molecular mass spectra of MSQs were characterized on a PE Biosystems (Framingham, MA) Voyager Biospectrometry workstation, using a 337 nm nitrogen laser, 20 kV acceleration voltage, and a 1.2 m flight tube. The different MSQs were deposited on a graphite plate substrate (instead of an organic matrix) to absorb the laser energy for desorption and ionization of the MSQ analyte.

Thermogravimetric Analysis (TGA). TGA measurements were performed on a TGA 2910 (TA Instruments) with the sample in an inert nitrogen atmosphere. Prior to testing, the samples were dried at 60 °C under vacuum and then thermally ramped in the TGA to 500 °C at a heating rate of 10 °C/min.

Specular X-ray Reflectivity (SXR) and X-ray Porosimetry (XRP). SXR measurements were performed on a Philips model X'PERT MRD reflectometer using a finely focused Cu−Kα radiation (λ = 1.54 Å) source. The reflectivity was collected at room temperature to determine the critical angle of the sample in a vacuum. Next, the sample chamber was saturated with toluene vapor at 25 °C for 1 h after which the reflectivity was measured again. The difference in the critical angle with and without toluene determines the porosity and wall density of the material between the pores. Precision out-of-plane CTE measurements were derived from thickness measurements as a function of temperature using the SXR technique. The thickness of each film is determined from the periodicity of the interference fringes. PMSQ films were placed in a specially designed vacuum chamber and the thickness was measured at 25, 75, 125, and 175 °C. Each film was first held at 175 °C under a vacuum of 10^{-6} Pa for 1 h and then cooled to 25 °C prior to the CTE measurement. After completing a set of measurements up to 175 °C, the samples were cooled back to 25 °C and the measurements were repeated in order to confirm reversible expansion and contraction behavior.

Results and Discussion

It is generally understood that for MSQ-type materials to form film structures with required optical and mechanical properties, the material should be oligomerized or polymerized before being deposition onto a substrate. Once thin films are deposited onto a substrate they are typically exposed to high temperature vitrification process up to 400 °C to complete the secondary cross-linking reaction. The physical properties of the final films are determined by the microstructure after vitrification, which in turn depend on the initial microstructure and the structural transformation during thermal vitrification. In this regard, we first investigated the initial microstructures of the MSQ prepolymers and then characterized the structural transformation during vitrification process. It will be shown that the physical film properties are significantly dependent upon the initial microstructure of MSQ prepolymers.

The initial microstructures of the oligomeric MSQs with different reaction times are first examined by SEC. The SEC traces for initial MSQ-1 (prepared at 40 °C for 30 min) and MSQ-2 (prepared at 40 °C for 24 h) samples are shown in Figure 1. MSQ-1 exhibits a single and narrow molecular mass distribution peak, whereas a broad bimodal distribution is observed for MSQ-2, indicating that the average molecular mass increases with the reaction time. ^{1}H NMR measurements of the MSQ-1 and MSQ-2 indicate that most of functional end groups are silanol (Si−OH) groups and higher amount of silanol groups are detected for MSQ-1. Overall, increase of molecular mass and decrease of the amount of silanol groups are observed by increasing the reaction time.

The SEC measurements in Figure 1 semiquantitatively indicate differences in the molecular structure of the different reaction products. GPLDI-TOF MS measurement can be used to help quantify these differences. Previously, we used GPLDI-TOF MS to identify the reaction products of methyltriethoxysilane (MTES).[20] A rapid hydrolysis of the Si−OC_2H_5 groups is followed by an intermolecular condensation reaction between two silanol groups, resulting in partially hydrolyzed linear oligomers with a wide range of number of Si-atoms.

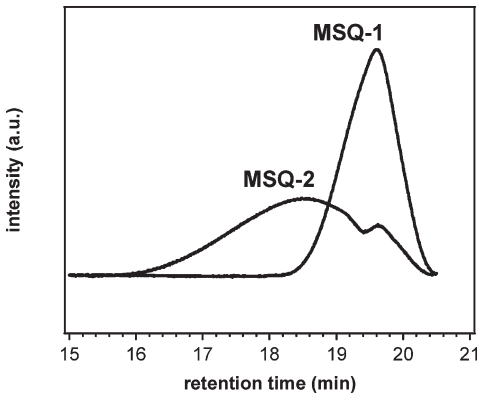

Figure 1. SEC chromatograms of initial MSQ-1 and MSQ-2 samples. MSQ-1 was prepared by carrying out the reaction at 40 °C for 30 min, and MSQ-2 was obtained by reacting at 40 °C for 24 h.

The previous GPLDI-TOF MS measurements revealed various short ladder-type branched structures with four to six silanol groups per oligomer. The GPLDI-TOF MS characterization of MSQ-1 (Figure 2a) is in good agreement with the previous result, indicating that the major products in the initial stages of the reaction are ladder-type branched structures with silanol end groups. The insets to Figure 2a show the molecular structures that correspond to the different molecular mass peaks. In addition to the predominance of the ladder-type branched structures, there are also some incomplete or partial cage-type structures, such as $T_7(OH)_3$ (m/z 519-($+Na^+$) and 535($+K^+$)), $T_8(OH)_2$ (m/z 576($+Na^+$) and 594($+K^+$)), and $T_9(OH)_3$ (m/z 654($+Na^+$) and 670-($+K^+$)) in the mass spectrum of MSQ-1. The differences here between the MTMS reaction products and the previous study of the MTES can be understood in terms of the relatively faster hydrolysis of $Si-OCH_3$ groups in MTMS compared with $Si-OC_2H_5$ groups in MTES.[20]

Intramolecular cyclization of oligomeric ladder-type structures in MSQ-1 at longer times (i.e., MSQ-2) leads to the formation of incomplete cage structures with two or three silanol groups, as observed in the GPLDI-TOF MS mass spectrum of MSQ-2 (see Figure 2b). The insets to Figure 2b again display the molecular structures associated with discrete peaks in the mass spectrum. By comparing the structures in Figure 2a and b, it becomes apparent that small ladder-type branched structures formed at short reaction times tend to wrap up into more cagelike architectures at longer times. Note that these "cyclization reactions" of the ladder-type structures occur through a condensation reaction that decreases the atomic mass of the molecule by 18.02 u (mass of a water molecule). One must be careful in interpreting this small difference given that both sodium and potassium adducts, which differ in molecular mass by 16.1 u, are generated in GPLDI-TOF MS. Hence, it should be always taken into account that the sodium adduct peak of the hydrolyzed structure and the potassium adduct peak of the dehydrolyzed product overlap within the resolution of the equipment used in this study. For example, the sodium adduct peak and the potassium adduct peak of $T_9(OH)_3$

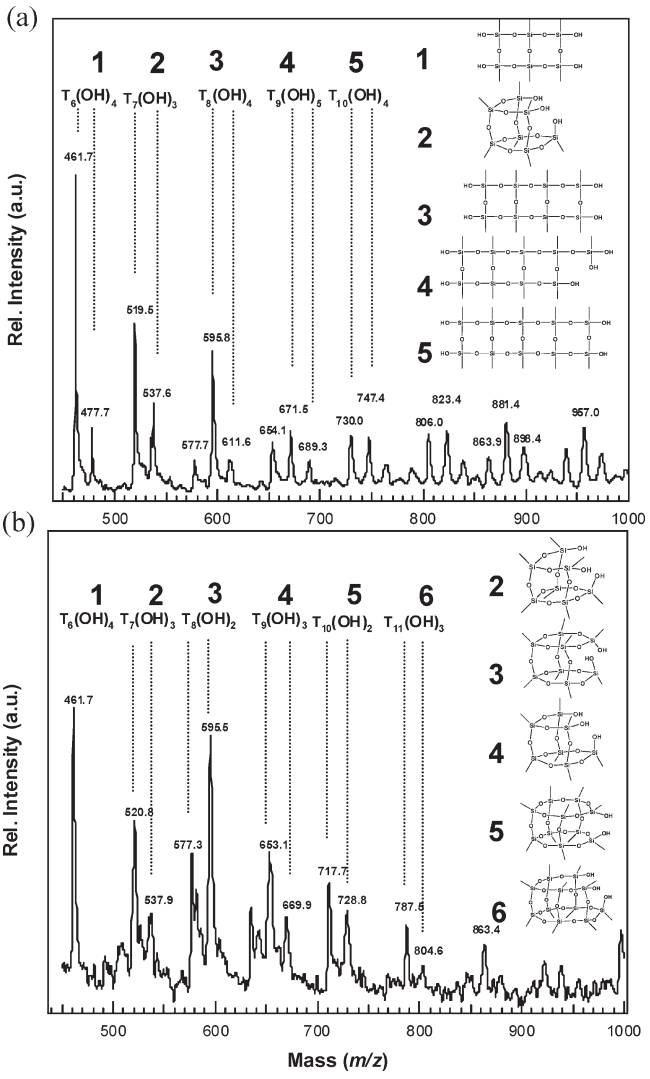

Figure 2. Mass spectrum of (a) MSQ-1 and (b) MSQ-2 in the molecular mass region below 1000 Da. The major microstructures for each MSQ molecular mass are schematically drawn.

are observed at m/z of 654.1 and 671.5, respectively, in the mass spectrum of the MSQ-1 product. Peaks from the precursor of $T_9(OH)_3$, the branched ladderlike structure $T_9(OH)_5$, are observed at m/z of 671.5 and 689.3, respectively. These peaks are shifted by 18 u to lower masses in the spectrum of MSQ-2, which indicates that a ladderlike branched structure, $T_9(OH)_5$, is converted to a incomplete cage structures, $T_9(OH)_3$, by an intramolecular condensation reaction with a byproduct of a H_2O molecule. The intensities of incomplete cage peaks, such as $T_7(OH)_3$, $T_8(OH)_2$, $T_9(OH)_3$, $T_{10}(OH)_2$, and $T_{11}(OH)_3$, are more pronounced in the low molecular mass species for the spectrum of MSQ-2 (see Figure 2b), indicating the formation of cage-type microstructures by consecutive intramolecular cyclization reactions at longer reaction times. The evolution or "wrapping up" of the low molecular mass, ladder-type molecules into closed cage-type structures is schematically depicted in Figure 3.

The microstructure evolution of MSQ in the high molecular mass region, over 1000 u, is explored by introducing more vigorous reaction conditions (prepared at

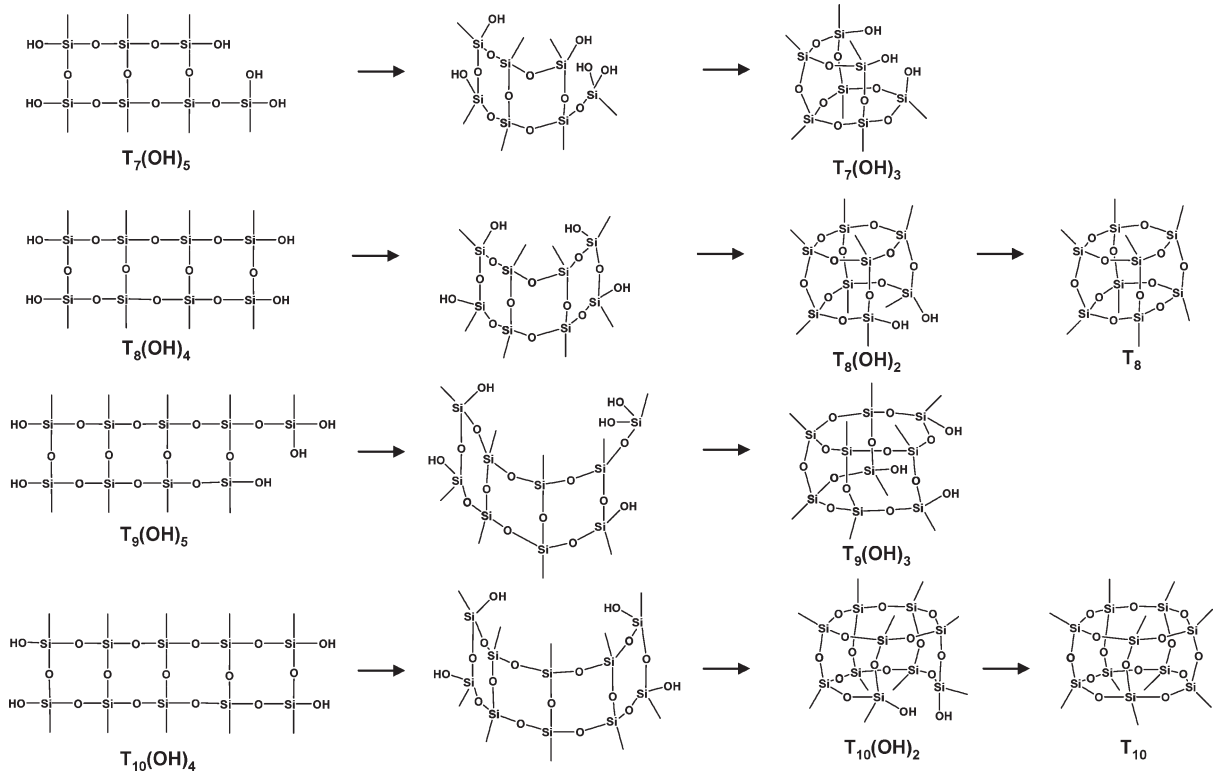

Figure 3. Schematic evolution process for constructing the cage-type MSQs.

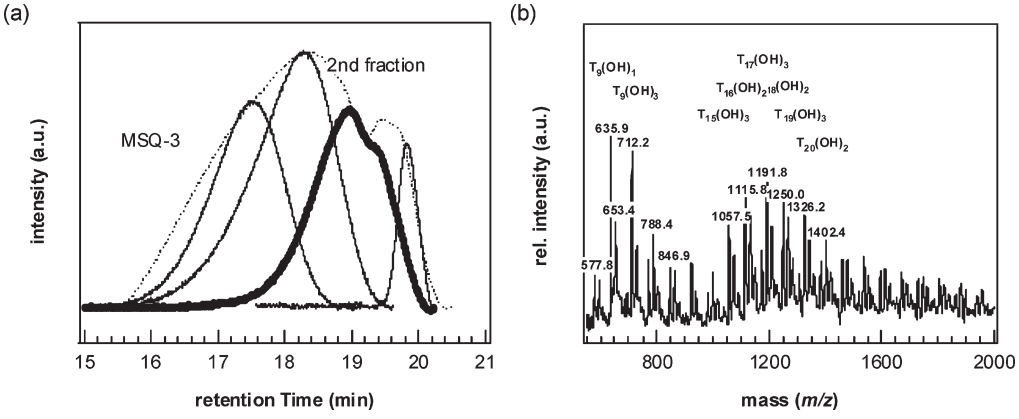

Figure 4. (a) SEC chromatograms of MSQ-3 before and after fractionation and (b) GPLDI-TOF mass spectrum of the second fraction (denoted by bold line) of MSQ-3.

60 °C for 24 h) for the MSQ-3 sample. The weight-average molecular weight of the MSQ-3 is determined as approximately 9000 with a large polydispersity index (PDI) of 4.59 from the calibration curve of the polystyrene standards. Since high molecular mass MSQs typically have a PDI that is often greater than two, it is difficult to quantify their distributions by conventional mass spectrometry. We can overcome this by fractionating the MSQ-3 into four sequential fractions of molecular mass using two connected mixed-bed columns. The SEC trace of the initial MSQ-3 is compared with fractionated aliquots in Figure 4a. The different elution times for the different fractions reflect the deconvolution of the molecular mass distribution for the initial MSQ-3. The GPLDI-TOF MS spectrum of just the second fractionation of MSQ-3 is shown in Figure 4b. As with the MSQ-2, there is strong evidence for closed cage structures in the lowest molecular mass regions of Figure 4b. For molecular masses larger than 700 u, the spectra are consistent with a mixture of ladder-type branched species ($T_n(OH)_m$, $n > 14, m > 3$) and open cage-type structures ($T_n(OH)_m$, $n > 13, m < 3$). It is worth emphasizing that the products in the low molecular mass regime for MSQ-3 mainly consist of cage-type structures, whereas a mixture of ladder-type branched and open-cage structures is observed in the molecular mass portion higher than 1000 u. This indicates a strong tendency to form polyhedral cage structures in the low molecular mass portion, where the number of Si atoms per cage-type structures ranges from 8 to 12.

Intramolecular cyclizations were reported as the dominant reaction products in the hydrolytic condensation of

propyltrimethoxysilane (PTMS) and *iso*-butyltrimethoxysilane (*i*-BTMS).[28] In these systems, the propensity for the formation of chain extension or ladder-type species is small. The dominance of cyclization over branching or chain extension leads to the formation of open and perfect cages, including the T_8, T_{10}, T_{14}, and T_{16} structures, at relatively short reaction times and in low molecular mass portions of the PTMS and *i*-BTMS systems. In contrast, the rates of the intramolecular cyclization and intermolecular chain-extension are competitive in the early stages of the hydrolytic polycondensation of MTMS. This is confirmed here from the GPLDI-TOF MS and SEC data presented above. Only at much longer reaction times do the intramolecular cyclization reactions transform the initial ladder-type branched structures into cage-type microstructures with the 12 or less Si-atoms. As mentioned previously, the perfect cage structures completely lack the silanol functionality and become insoluble in the reaction mixture. In fact, the perfect cages become insoluble in the acidic reaction mixtures. This is confirmed by the observation of white precipitates in the reaction products for MSQ-2 and MSQ-3. We have collected these precipitates by centrifugation and characterized by FT-IR. The results indicate that they are mainly comprised of the octametyl-T_8 perfect cages. In contrast, no precipitates are observed in the MSQ-1 reaction product. Consistent with the GPLDI-TOF MS and SEC data, the reaction products in MSQ-1 are low molecular mass partial cages and branched structures with high silanol content, readily soluble in the reaction product mixture. Also, it is important to note that the results for the MSQ-2 and MSQ-3 samples, obtained after the longer reaction times, show that not all of the ladder-type branched structures become wrapped up into cagelike structures. This is confirmed by the fact that the average molecular mass of MSQ continues to increase with reaction time, rather than reaching a plateau value to be expected if all the species transformed into nonreactive perfect cages. Therefore, the important result is that both the intramolecular cyclization and intermolecular chain-extension reactions remain active throughout the hydrolytic condensation of MTMS.

The FT-IR spectra for the initial MSQ-1 and MSQ-2 are shown in Figure 5. The bands observed near 930 cm^{-1} are assigned to the Si−OH stretching vibration while the broad peak around 3300 cm^{-1} reflects O−H stretching mode. Other bands of particular interest include the various Si−O−Si stretching modes in the range of 1000−1200 cm^{-1}. These can be broken down into two asymmetric Si−O−Si stretching bands, $\nu_{ring\text{-}asym}$ at about 1100 cm^{-1} and $\nu_{ring\text{-}sym}$ at about 1050 cm^{-1}. As reported previously, the branched ladder-type and open cage structures exhibit both $\nu_{ring\text{-}asym}$ and $\nu_{ring\text{-}sym}$ modes, but the intensity of $\nu_{ring\text{-}asym}$ absorption band at about 1100 cm^{-1} is stronger for open-cage structures. In contrast, the intensity of $\nu_{ring\text{-}sym}$ absorption band at about 1050 cm^{-1} is stronger for ladder-type branched structures.[26] In this regard, the FT-IR spectra of the initial MSQ-1 and MSQ-2 samples are in good agreement with the interpretation of the GPLDI-TOF MS data. MSQ-1, for which the major component is the ladder-type branched structures, exhibits a broad single peak centered at 1031 cm^{-1} while two separate peaks at 1020 and 1095 cm^{-1} are evident for MSQ-2. The fact that the FT-IR data are consistent with and well-correlated to the GPLDI-TOF MS data is very important. This is because the GPLDI-TOF MS method can only be used to characterize relatively low molecular mass oligomers but cannot be used to characterize the molecular structure of the cured MSQ films as they are thermally vitrified into a highly cross-linked network. Therefore, one has to exclusively rely on the FT-IR method in order to characterize the MSQ films as a function of vitrification temperature, as described below.

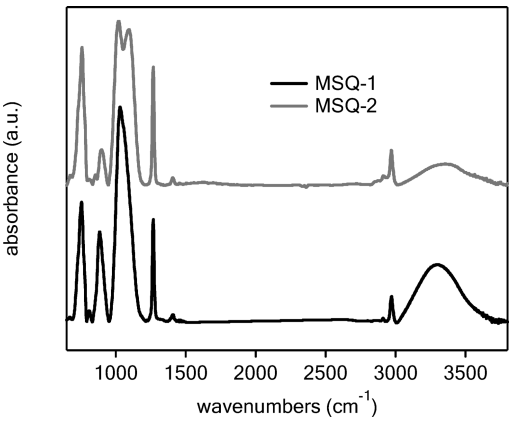

Figure 5. FT-IR spectra of (a) initial MSQ-1 and (b) MSQ-2.

The secondary condensation (curing) of the MSQ-1 and MSQ-2 oligomers into the cross-linked network was monitored as a function of curing temperature using FT-IR. Films were heated at a rate of 3 °C/min to 60, 150, 300, or 430 °C and allowed to equilibrate at each temperature for 10 min in vacuum before collecting the FT-IR data. Figure 6 shows the FT-IR spectra for both the MSQ-1 and MSQ-2 films at each temperature. The MSQ-1 film annealed at 60 °C shows a broadband centered at 1100 cm^{-1} with a weak shoulder at 1040 cm^{-1}. The MSQ-2 film heated to 60 °C shows two discrete bands at 1040 and 1114 cm^{-1}. Compared with the FT-IR spectra for the initial reaction products, the relative peak intensities indicate an increase in the population of open cage structures as a result of the secondary condensation reactions. Upon comparing the results of MSQ-1 and MSQ-2 films, the dominance of the broad peak at 1100 cm^{-1} in the MSQ-1 and the larger hydroxyl content reflected in the peak around 3300 cm^{-1} indicates that the ladder-type branched structures are still more prevalent in the MSQ-1 film.

Significant structural changes occur in the MSQ-1 film when the secondary condensation reactions take place as the temperature increases from 60 to 300 °C. Above 300 °C, the reaction appears to be almost completed. The spectra at both 300 and 430 °C are very similar. In the MSQ-1 film, the broad single peak at 1100 cm^{-1} in the 60 °C-cured film

(28) Kim, H.-J.; Lee, J.-K.; Kim, J.-B.; Park, E. S.; Park, S.-J.; Yoo, D. Y.; Yoon, D. Y. *J. Am. Chem. Soc.* **2001**, *123*, 12121.

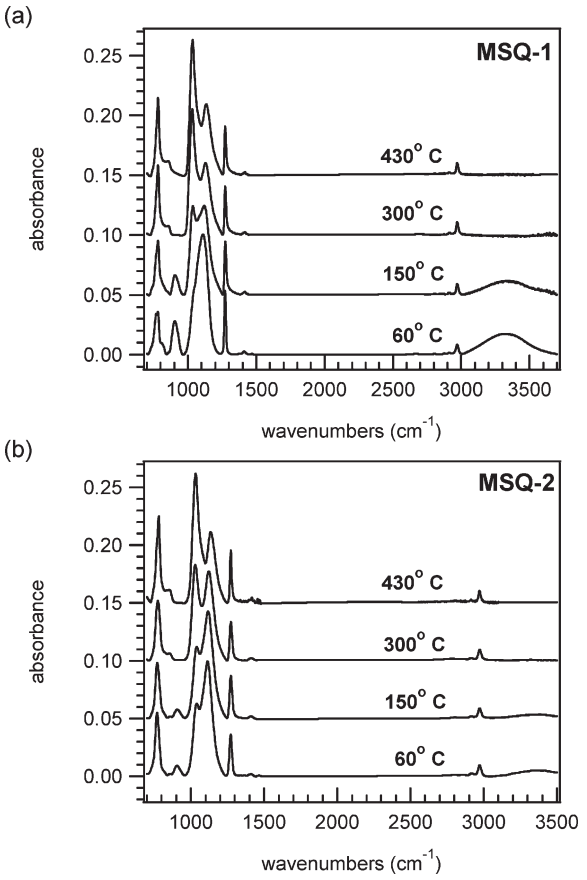

Figure 6. Transmittance FT-IR spectra of the (a) MSQ-1 and (b) MSQ-2 films prepared at 60, 150, 300, and 430 °C.

evolves into two separate peaks at 1035 and 1120 cm^{-1} as the film is heated to higher temperatures. The intensity of 1035 cm^{-1} peak from the branched structure increases with temperature, while the intensity of the peak for the partial cagelike structures at 1120 cm^{-1} decreases. In the MSQ-2 film, most of the thermal transformation occurs in the temperature range from 150 to 430 °C. Between 60 and 150 °C, the intense peak at 1114 cm^{-1} is shifts slightly to 1116 cm^{-1}, which corresponds to the perfect T_8 cages, while the position and intensity of the 1040 cm^{-1} peak is maintained. The dominant microstructures at 150 °C in the MSQ-2 are characterized as partial cages having two or three Si−OH groups in conjunction with perfect T_8 cages. Above 150 °C, the intensity of the perfect cage peak (1116 cm^{-1}) decreases significantly and the dominant peak shifts to 1122 cm^{-1}. Although the initial microstructures in the as-cast MSQ-1 and MSQ-2 are distinctly different, it is interesting that the final FT-IR spectra of the fully cured films at 430 °C are quite similar, with only slight difference in the intensity of the peak around 1100 cm^{-1}. As will be discussed below, there are, however, very large differences in the physical properties of the fully vitrified MSQ films.

The thermal evolution of the condensation reaction products for the MSQ films was monitored by TGA thermograms as shown in Figure 7. Both MSQ-1 and MSQ-2 show a mass loss upon heating to high temperature. One origin for this mass loss is the evolution of H_2O through the condensation of the silanol groups that leads

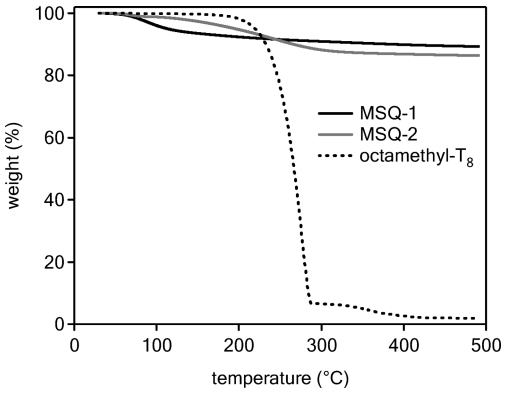

Figure 7. TGA thermograms of MSQ-1 and MSQ-2. The result for octamethyl-T_8 (cubic octamer) is also shown for the purpose of comparison. The inset is a magnification of the important temperature region.

to the Si−O−Si bond formation. In the MSQ-1, most of this mass loss occurs between 60 and 130 °C, consistent with the condensation reaction mechanism. However, the thermally induced mass evolution in the MSQ-2 shows a two-step process. The mass loss first becomes significant above 60 °C, consistent with the condensation of the silanols as in the MSQ-1 films. However, a dominant second process occurs above approximately 200 °C. For comparison, Figure 7 also displays the TGA result of a pure octamethyl-T_8 cube compound, which clearly shows that the T_8 cubes sublime above 200 °C. From this result, we conclude that the second mass loss mechanism (near 200 °C) in the MSQ-2 is evaporation or sublimation of isolated perfect T_8 cages. The presence of these perfect cages in the MSQ-2 is confirmed by both the FT-IR and the GPLDI-TOF spectra. The loss of these cages above 200 °C is consistent with the XRD and TGA results of MSQ-2 films and the TGA result of octamethyl-T_8 molecules reported elsewhere.[29] Therefore, the larger mass loss of MSQ-2, in spite of the smaller amount of Si−OH content (12.9 mol %) compared with that of MSQ-1 (20.3 mol %), is interpreted as arising from the loss of the perfect cage structures by sublimation. This interpretation also supports the final film properties after thermal vitrification. After heating MSQ-1 up to 430 °C, the final film is transparent and defect-free. The MSQ-2 film is initially transparent but becomes opaque upon heating past 100 °C and generates many visible defect sites after full vitrification at 430 °C. The loss of low molecular-mass cage structures is further confirmed by the changes in the X-ray powder diffraction results for the MSQ-1 and MSQ-2 films as reported previously.[27] Sharp diffraction peaks indicating the presence of crystalline structure are observed only for the MSQ-2 film cured at 150 °C. All the other films exhibit broad amorphous halos indicating a lack of any ordered structure. The Bragg angles for the crystalline peaks in the MSQ-2 cured at 150 °C correspond to the *d*-spacings of 0.79 and 0.42 nm. These peaks are consistent with the crystalline packing of the perfect octamethyl-T_8 structures. As already mentioned, the

(29) Bolln, C.; Tsuchida, A.; Frey, H.; Mulhaupt, R. *Chem. Mater.* **1997**, *9*, 1475.

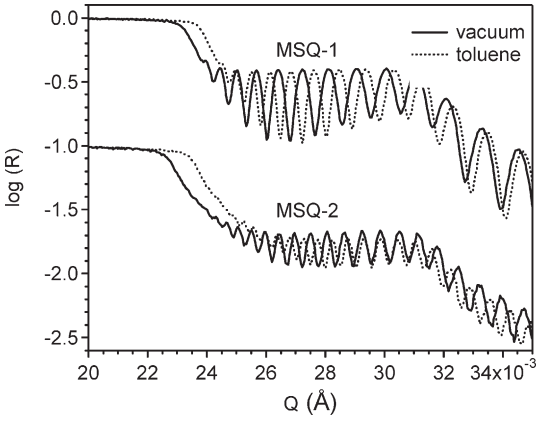

Figure 8. SXR curves of fully vitrified MSQ-1 and MSQ-2 films. The curves are offset for clarity. The relative standard uncertainty in the SXR intensities is less than the line widths: (solid line) X-ray reflectivity curve recorded in vacuum, (dotted line) X-ray reflectivity curve after saturation with toluene vapor.

perfect cage structures are nonreactive and cannot be chemically bonded to the MSQ network. Therefore, the fact that the crystalline X-ray peaks disappear for the films cured at temperatures above 150 °C confirms that the perfect cages are driven out of the film at elevated temperatures.

To investigate the effect of different microstructures of initial MSQs on the physical properties of the fully vitrified MSQ films, we evaluated the coefficients of thermal expansion (CTEs) by utilizing specular X-ray reflectivity (SXR) measurements. For this purpose, the precise thicknesses of fully vitrified films were determined by fitting SXR curves collected at 25, 75, 125, and 175 °C, and the temperature dependence of the film thickness yielded the out-of-plane CTE. Additionally, we used a variant of SXR, known as X-ray porosimetry (XRP), to quantify the density and intrinsic porosity of the different vitrified MSQ films. XRP is a combination of specular X-ray reflectivity (SXR) with the mechanism of capillary condensation; details of the experimental setup and measurement procedures are described elsewhere.[30−32]

Figure 8 shows the SXR data for the fully vitrified MSQ-1 and MSQ-2 films both in vacuum and after the intrinsic matrix pores have been filled by the capillary condensation of toluene vapor. The data are presented as the logarithm of the ratio of the reflected X-ray intensity (I) normalized by the incident beam intensity (I_0) versus the wave vector, Q ($Q = (4\pi/\lambda)\sin\theta$), where θ is the grazing incident angle of the X-ray beam. As the angle of incidence of X-ray increases, there is a sharp drop in the reflected intensity as the X-ray beam begins to penetrate the film at the so-called critical angle. The wave vector for this critical angle (Q_c) is proportional to average electron density of the film through $Q_c^2 \propto \rho_{electron}$. The electron density determined from Q_c can be converted into mass density through the atomic composition. The critical angle of the film in the toluene environment increases in both MSQ-1 and MSQ-2 films, due to the capillary condensation of toluene in the accessible pores. Since the density of the toluene is known, a simple two-phase model of mixtures comprised of voids within a homogeneous solid wall material can be applied. This provides two unknowns, the porosity, P, and the wall density, ρ_{wall}. The critical angles measured in vacuum and in the presence of toluene vapor reveal the average density of the evacuated film, $\rho_{average}$, and the solvent saturated film, $\rho_{saturated}$. P and ρ_{wall} can then be determined by simultaneously solving the two equations:

$$\rho_{average} = \rho_{wall} \times (1 - P)$$

$$\rho_{saturated} = \rho_{solvent} \times P + \rho_{wall} \times (1 - P)$$

where the $\rho_{solvent}$ is the average mass density of toluene, taken to be 0.865 g/cm^3 at room temperature. It should be noted that the ρ_{wall} is the average density of wall material and any unfilled pores smaller than the toluene molecule. These measurements reveal that the average density is greater for the MSQ-1 film compared with the MSQ-2 while the wall densities are nearly the same. The reported values are $\rho_{average} = (1.22 \pm 0.05)$ g/cm^3 [The error bars presented throughout this manuscript indicate the relative standard uncertainty of the measurement.] and $\rho_{wall} = (1.30 \pm 0.05)$ g/cm^3 for MSQ-1 and $\rho_{average} = (1.17 \pm 0.05)$ g/cm^3 and $\rho_{wall} = (1.29 \pm 0.05)$ g/cm^3 for MSQ-2. Consistent with the lower average density, a higher intrinsic porosity of (9.7 ± 1.0) % by volume was measured for MSQ-2 film as compared with (6.3 ± 1.0) % by volume for the MSQ-1. The higher porosity and lower average film density in the MSQ-2 is entirely consistent with the sublimation of the perfect T_8 cages from the film upon vitrification, which leaves behind additional porosity.

Figure 9 shows the temperature-dependence of film thicknesses, determined from the SXR data for the fully cured MSQ-1 and MSQ-2 films. Here, the thickness at each temperature is determined by Fourier transform methods, converting the fringe periodicity to a model-independent film thickness.[33] The reflectivity data can also be modeled using a least-squares fitting routine to extract film thickness.[34] Both methods have sufficient sensitivity to the angstrom level variations in the film thickness, and the CTEs from both methods were consistent with each other; therefore, we took the average value in this manuscript. There is a remarkable difference in the CTEs obtained for the two different MSQ films. The CTE value of MSQ-1 of (104.6 ± 3.6) × 10^{-6}/°C is significantly smaller than that for MSQ-2 of (278.1 ± 7.4) × 10^{-6}/°C. These values fall between the CTE values recently reported for commercialized MSQ systems of 200 × 10^{-6}/°C determined by using ellipsometry,[35] so the CTEs observed here seem reasonable for an MSQ type material. However, the large difference in CTEs between the

(30) Lee, H. J.; Soles, C. L.; Liu, D. W.; Bauer, B. J.; Lin, E. K.; Wu, W. L.; Grill, A. *J. Appl. Phys.* **2004**, *95*, 2355.
(31) Bouldin, C. E.; Wallace, W. E.; Lynn, G. W.; Roth, S. C.; Wu, W. L. *J. Appl. Phys.* **2000**, *88*, 691.
(32) Wu, W.-L.; Liou, H.-C. *Thin Solid Films* **1998**, *312*, 73.
(33) Parratt, L. G. *Phys. Rev.* **1954**, *95*, 359.
(34) Anker, J. F.; Majkrzak, C. F. *SPIE Proc.* **1992**, *1738*, 260.
(35) Oh, W.; Hwang, Y.; Park, Y. H.; Ree, M.; Che, S.-H.; Char, K.; Lee, J. K.; Kim, S. Y. *Polymer* **2003**, *44*, 2519.

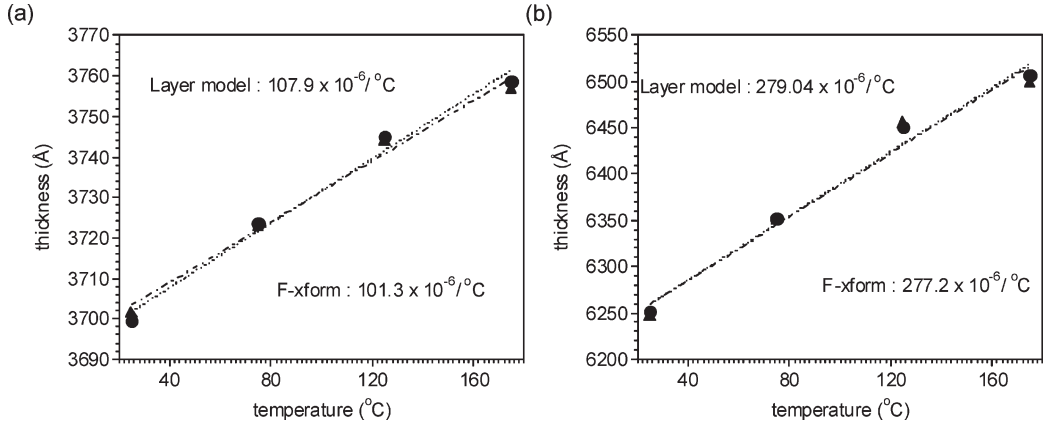

Figure 9. Thickness of (a) MSQ-1 and (b) MSQ-2 films as a function of temperatures. The thicknesses at different temperatures determined by the Fourier transform method (circle) and least-squares fitting of the reflectivity curves (triangle) are hardly distinguishable.

MSQ-1 and MSQ-2 is very striking. Apparently, the differences in the microstructures of the initial reaction products have a profound impact on the CTE of the fully cured films.

The XRP data show that the average density of the MSQ-2 film was slightly lower, but this is directly offset by the slightly higher porosity in the MSQ-2. So the physical density of the wall material separating the pores is about the same. Each MTMS monomer initially contains trifuctional reaction sites and therefore has the potential to form 3 covalent bonds. As the reaction process proceeds, small molecular mass MSQs start to form, as shown in the insets to Figure 2. The first reaction products start out as low molecular mass ladder-type molecules. At longer reaction times these low molecular-mass branched ladder-type structures have propensity to assemble into partial and/or perfect cage structures in reaction solutions. As one spin-casts these prepolymers into solid films, the intermolecular cross-link density of the resulting network upon secondary condensation will depend critically on the silanol content of the oligomers. Since the branched structures of MSQ-1 have a higher silanol content (20.3 mol %) as compared with MSQ-2 films (12.9 mol %) which contain a higher fraction of cage-like structures, we propose that this high cross-link density is responsible for the smaller CTE for the vitrified MSQ-1 films. In reality, this explanation is still too simplistic because we ignore the consequence of the sublimed cage structures in the vitrified MSQ-2 films. In fact the higher molecular mass MSQ-3 exhibits a CTE between those of MSQ-1 and MSQ-2 with comparable film quality of MSQ-1. This can be understood in terms of the microstructure of the initial prepolymers. The more vigorous reaction conditions for MSQ-3 leads to an increased portion of the higher molecular mass species and minimizes the oligomeric species below 1000 Da. This also minimizes the fraction of species which can form oligomeric cagelike molecules during the thermal vitrification process and thus results in the high quality film. Therefore, increasing the molecular mass of the initial MSQ prepolymer or eliminating low molecular mass species by fractionation is another effective way to improve the film quality of MSQ materials. Although the physical properties of the film prepared from higher molecular mass MSQ (MSQ-3) are comparable with low molecular mass analog (MSQ-1), the increase of molecular mass always leads to a lower silanol content (9.0 mol % for MSQ-3 compared with 20.3 mol % for MSQ-1). These materials are often used as candidates for highly porous low-k dielectrics for semiconducting applications, and a larger silanol content is attractive to further decrease the dielectric constant by incorporating nanoscale pores using thermally degradable pore-generator materials; silanols help disperse a larger amount of porogen into the material. So despite the comparable film quality of the MSQ-1 and MSQ-3, generating porosity levels as high as 30% were achieved using MSQ-1, but only 10−15% of porosity was created without degrading the film quality for MSQ-3.

In conclusion, our measurements show that controlling the reaction conditions used to prepare the MSQ prepolymers is extremely important for optimizing the physical properties of the final vitrified film. Specifically, it is important to understand how the cross-linked microstructure evolves from the initial monomers through the oligomeric prepolymer stage before transforming into the fully vitrified material. FT-IR spectroscopy measurements on the fully vitrified films alone do not provide the critical insight into the potential breadth of physical properties achievable with these materials. In many applications, such as interlayer dielectric insulators, it is desirable to minimize the coefficient of thermal expansion, minimize the defect density, and maximize the mechanical properties of the films. This can be achieved by minimizing the formation of low molecular-mass partial or perfect cage structures, which degrade the final vitrified film by (1) decreasing the effective cross-link density of the material and (2) exhibiting a propensity to sublime from the film at elevated temperatures. Therefore, one can tailor the microstructure of a MSQ-type material by controlling the reaction conditions for preparing the prepolymers, which has a direct impact on the final film quality. Decreasing the probability of forming

isolated cages and maximizing the cross-linking density of the vitrified films are the most effective ways to improve the final film quality.

Note Added after ASAP Publication. There was a minor text error in the Results and Discussion section in the version published ASAP January 7, 2010; the corrected version was published ASAP January 8, 2010.

Acknowledgment. We thank Profs. J.-K. Lee and H.-J. Kim for the helpful discussions on this work. This work was supported in part by the Chemistry and Molecular Engineering Program of the Brain Korea 21 Project and the "System IC 2010 Project" of the Korean government. The authors also acknowledge the financial support from the National Institute of Standards and Technology Office of Microelectronics Programs.